

Distribution-based BRDFs

Michael Ashikhmin
Stony Brook University

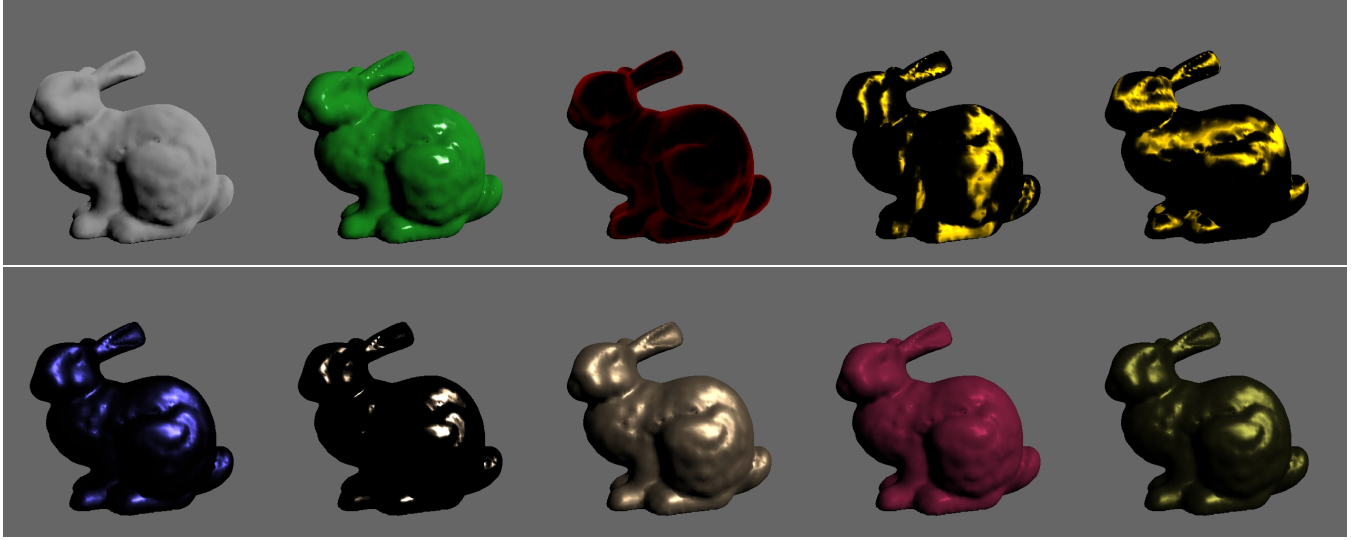


Figure 1: Various BRDFs generated with our model, all implemented in hardware. Analytic distributions, top row: uniform; Phong with extra Lambertian term; synthetic velvet; anisotropic Phong ($n_1 = 1, n_2 = 100$) with two different anisotropy axis orientation. Approximations for measured materials, bottom row (see Figures 5 and 8): metallic blue; nickel; pearl paint; resin; Christmas ball.

Abstract

The bidirectional reflectance distribution function (BRDF) formalism is commonly used in computer graphics to represent surface reflection properties. Although many BRDF models have been proposed, most do not possess at least some of the desirable practical properties. In this paper we present a simple and flexible model which satisfies many of these requirements. We show that the proposed model provides a good approximation for many real world materials, obeys basic physical restrictions, allows straightforward hardware implementation and provides for efficient sampling in a Monte-Carlo rendering system. A simple procedure to fit the model to BRDF measurement data is presented which suggests a simplified way of measuring surface reflection.

Keywords: BRDF, reflection measurement, rendering, importance sampling, microfacet models

1 Introduction

For a material to be perceived correctly in a computer graphics image, the main characteristics of its interaction with incoming light

should be faithfully reproduced. Although many physical processes contribute to this interaction, surface reflection has rightfully received the most attention from computer graphics community since it is typically the most prominent effect visually. Physically-based rendering systems describe reflection behavior using the bidirectional reflectance distribution function (BRDF) $\rho(\mathbf{k}_1, \mathbf{k}_2)$ [Nicoledemus et al. 1977] which describes what fraction of light coming from a given direction \mathbf{k}_1 is reflected into some other direction \mathbf{k}_2 . All vector quantities appear in **bold** throughout the paper. Much research has concentrated on developing suitable mathematical models for, or direct measurement of, this four-dimensional function.

To most faithfully reproduce reflectance properties of real-world materials, several BRDF measurement systems for computer graphics have been designed both based on the classical goniorelectrometer approach [Greenberg et al. 1997] and, recently becoming more popular, using image-based techniques [Ward 1992; Marschner et al. 1999]. The quality and the amount of reflection data obtained with such systems has improved significantly in recent years [Matusik et al. 2003; Matusik et al. 2004]. However, it remains very difficult to obtain accurate and reliable data, especially in areas near grazing angles, and near the directions of backscattering and strong specular highlights. The measurement process itself remains laborious and time-consuming. Significant investment is typically necessary to build a measurement system.

A range of BRDF models from very simple [Phong 1975; Blinn 1977] to quite sophisticated [He et al. 1991; Stam 1999] has been proposed. As an alternative to measurement, parameters of such models can be adjusted for the best visual match with real materials in what is often a rather tedious process. Somewhat surprisingly, results obtained in this manner with even some of the simplest models are often sufficient to withstand the scrutiny of many of the most demanding visual effects applications. We believe that this is due to

two main reasons. First, the human visual system generally seems to be not very sensitive to the details of material appearance as long as its main features (such as overall color and the width of specular highlight) are reasonably accurately reproduced. Supporting this proposition, it was recently demonstrated [Matusik et al. 2003] that many common BRDFs can be projected into a relatively low dimensional space as well as represented by a linear combination of as few as 100 BRDFs [Matusik et al. 2004] without noticeable degradation in perceived material properties. Second, realistic illumination conditions, complex scene geometry and textures, all abundant in modern computer graphics, further mask any inaccuracies in the surface reflection representation.

Although generally accepted in the BRDF research community, these considerations, in our opinion, have not yet led to a sufficiently simple and flexible process of handling surface reflection in computer graphics. This is due to many difficult to enforce and sometimes contradictory requirements one would like to combine in a useful BRDF representation. Specifically, if possible, it is desirable for such a representation to:

- represent a significant number of real-world materials with sufficient accuracy for visual applications;
- use measured data and allow acquisition of the necessary information for existing materials quickly and easily;
- be able to model new materials from scratch, i.e., not rely exclusively on measured data;
- respect basic physical properties of non-negativity, reciprocity and energy conservation;
- allow efficient sampling in a Monte-Carlo rendering system;
- allow hardware implementation;
- be compact;
- have at least a semi-intuitive interpretation and be simple to use for non-BRDF experts.

A quick look at BRDF research literature reveals that no existing representation offers all these properties simultaneously. Using measured [Marschner et al. 1999] or simulated [Westin et al. 1992] data directly does not offer a compact solution. Recent systems based on decomposition of acquired data are quite complex. They typically target specific properties such as hardware implementation [Kautz and McCool 1999; McCool et al. 2001] or sampling efficiency [Lawrence et al. 2004] making sacrifices in other areas. With the exception of the Matuzik et al. [2003] system, modeling of novel materials is also difficult. While simple Phong-like models [Ward 1992; Ashikhmin and Shirley 2001] and early microfacet-based models [Torrance and Sparrow 1967; Cook and Torrance 1981] can be successful for many materials, they do not offer sufficient flexibility. This drawback is shared by most other models which are in many cases also not simple enough to be easily fit to experimental data, implemented in hardware, or offer efficient sampling schemes. This includes wave physics-based models [He et al. 1991; Stam 1999] as well as those specialized for relatively narrow, although important, classes of materials [Oren and Nayar 1994; Neumann et al. 1999]. Ashikhmin et al.'s microfacet-based model [2000] is the most flexible among analytic ones, but its mathematical form is likely to make fitting it to measured data particularly difficult. Lafortune et al. [1997] presented a technique which fits a sum of generalized Phong lobes to measured data. While successful for some materials, the method often fails to match more complex appearance and the non-linear fitting procedure can become unstable if more than two or three lobes are involved. For a more detailed review of the state of the art in BRDF research

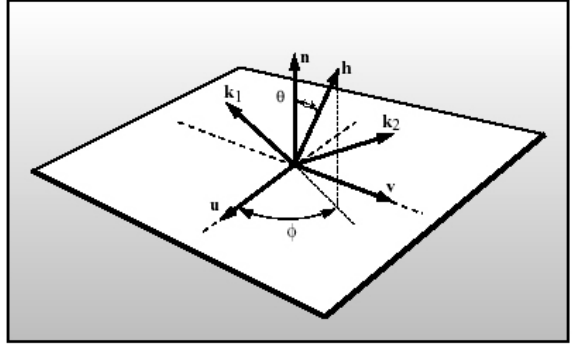


Figure 2: *Geometry of reflection. Halfvector \mathbf{h} has spherical coordinates (θ, ϕ) and lies in the plane defined by incident vector \mathbf{k}_1 and outgoing vector \mathbf{k}_2 .*

prior to 2001, the reader is referred to Ashikhmin et al.'s course notes [Ashikhmin et al. 2001].

This paper proposes a representation we call distribution-based BRDFs (d-BRDFs) which possesses the properties outlined above. In addition, it can lead to new economical procedures of measuring surface reflectance in the future. Section 2 presents the model and gives the intuition behind it. Section 3 describes a procedure for handling measured data. In Section 4 we describe a hardware implementation of the proposed model. We then demonstrate the efficiency of a Monte-Carlo sampling scheme based on the new model in section 5. We conclude with a discussion of limitations of our approach.

2 Distribution-based Reflection Model

We choose microfacet theory [Torrence and Sparrow 1967; Cook and Torrance 1981] as the general working framework. It assumes that the surface consists of a large number of small facets, each acting as a Fresnel mirror for incoming light according to the laws of geometric optics. Figure 2 shows the relevant geometry. We use notation (\mathbf{ab}) for the scalar product of vectors \mathbf{a} and \mathbf{b} . We assume that all vectors are normalized so the scalar product is just the cosine of the angle between the two vectors. For a facet to transfer light from the incoming direction \mathbf{k}_1 to the outgoing direction \mathbf{k}_2 , its normal direction has to coincide with the half-vector $\mathbf{h} = \text{normalize}(\mathbf{k}_1 + \mathbf{k}_2)$. Correspondingly, the distribution of normal directions of these facets $p(\mathbf{h})$ combined with the Fresnel term $F((\mathbf{kh}))$ and shadowing/masking effects on the surface are responsible for surface reflection. The theory was recently formulated for general distributions of microfacet normals [Ashikhmin et al. 2000]. It was noted that this distribution function had the greatest effect on the shape of reflection lobe. We take this observation to the limit and provide a simple expression for the BRDF where we directly use only $p(\mathbf{h})$, standard Fresnel fraction, and an overall scaling constant as characteristics of the surface.

We start from the anisotropic Phong model (also known as A&S model) [Ashikhmin and Shirley 2001] which, in addition to some desirable practical properties, was also demonstrated to perform well in fitting experimental data [Ngan et al. 2004] even though it was not originally intended for this purpose. We first note that by re-arranging the terms, we can write the specular part as:

$$\rho(\mathbf{k}_1, \mathbf{k}_2) = \frac{c_1 p_{\text{Phong}}(\mathbf{h}) F((\mathbf{kh}))}{(\mathbf{kh}) \max((\mathbf{k}_1 \cdot \mathbf{n}), (\mathbf{k}_2 \cdot \mathbf{n}))} \quad (1)$$

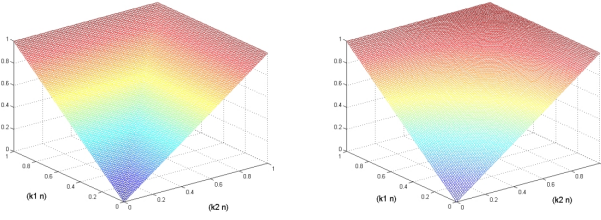


Figure 3: C_0 function $\max((\mathbf{k}_1 \mathbf{n}), (\mathbf{k}_2 \mathbf{n}))$ used in A&S model (left) and close in shape C_∞ bilinear patch $(\mathbf{k}_1 \mathbf{n}) + (\mathbf{k}_2 \mathbf{n}) - (\mathbf{k}_1 \mathbf{n})(\mathbf{k}_2 \mathbf{n})$, both having the same values on the boundary of the domain.

where $p_{Phong}(\mathbf{h})$ is anisotropic Phong function normalized so that it integrates to one over hemisphere of \mathbf{h} directions and c_1 is an RGB scaling constant. One can see that in this form, the empirical A&S model can be interpreted as a variant of microfacet models with a particular microfacet distribution $p(\mathbf{h})$ and Fresnel term both explicitly present. Other terms ensure energy conservation and reasonable behavior of the model close to grazing angles. In “true” microfacet models, the shadowing/masking terms take on this responsibility.

The first and most important change which we make now is to allow an arbitrary normalized function $p(\mathbf{h})$ (with average \mathbf{h} vector in the direction of surface normal) instead of specific p_{Phong} . This change is in the spirit of [Ashikhmin et al. 2000] but preserves a much simpler mathematical formulation. Second, we replace C_0 continuous term $\max((\mathbf{k}_1 \mathbf{n}), (\mathbf{k}_2 \mathbf{n}))$ with $(\mathbf{k}_1 \mathbf{n}) + (\mathbf{k}_2 \mathbf{n}) - (\mathbf{k}_1 \mathbf{n})(\mathbf{k}_2 \mathbf{n})$. This modification ensures greater continuity and removes the banding artefacts of the A&S model which can appear in some situations. The specific shape of new term represents a bilinear patch with the same “boundary conditions” as the original \max term, see Figure 3. Dropping the (\mathbf{kh}) term was found to produce a better overall appearance match to real-world materials (see Section 3). We therefore arrive at

$$\rho(\mathbf{k}_1, \mathbf{k}_2) = \frac{cp(\mathbf{h})F((\mathbf{kh}))}{(\mathbf{k}_1 \mathbf{n}) + (\mathbf{k}_2 \mathbf{n}) - (\mathbf{k}_1 \mathbf{n})(\mathbf{k}_2 \mathbf{n})} \quad (2)$$

In agreement with our assertion that $p(\mathbf{h})$ has the largest impact, we found that the resulting appearance is not very sensitive to the exact form of the expression in the denominator. Similarly, instead of the full expression for the Fresnel term, we use Schlick’s simple polynomial approximation [1994]:

$$F((\mathbf{kh})) = r_0 + (1 - r_0)(1 - (\mathbf{kh}))^5 \quad (3)$$

where r_0 is reflectance at normal incidence.

2.1 General properties of the model

For any non-negative distribution $p(\mathbf{h})$ the model is clearly non-negative and reciprocal. The distribution directly affects the shape of highlight which allows easy and intuitive modeling of its shape. Note that this is at most a 2D function (1D for isotropic surfaces) compared to the cumbersome four (three for isotropic) dimensions of full BRDFs. Although there is no distribution which exactly corresponds to a Lambertian BRDF, setting $p(\mathbf{h}) = \text{const}$ (and $F = 1$) results in surfaces very close to Lambertian in appearance (see the first image on Figure 1) making it possible to handle diffuse reflection within the same framework in most cases. The energy

conservation condition states that for any \mathbf{k}_1 we should have

$$\int \rho(\mathbf{k}_1, \mathbf{k}_2)(\mathbf{k}_2 \mathbf{n}) d\omega_{\mathbf{k}_2} \leq 1 \quad (4)$$

We substitute ρ from equation 2 and transfer the integration into the domain of half-vectors noting that [Torrence and Sparrow 1967] $d\omega_{\mathbf{k}_2} = 4(\mathbf{k}_1 \mathbf{h}) d\omega_h$. Extending the new integral over the complete hemisphere of \mathbf{h} directions and noting that the denominator of equation 2 is not less than $(\mathbf{k}_2 \mathbf{n})$ and $F \leq 1$, we arrive at a sufficient condition

$$4c \int p(\mathbf{h})(\mathbf{k}_1 \mathbf{h}) d\omega_h \leq 1 \quad (5)$$

Since p is normalized, a universal, although very loose, constraint to ensure energy conservation is $c \leq 1/4$. A much better (still conservative) bound for a specific distribution can be obtained by evaluating the maximal value of the integral in 5. Note that for typical single specular highlight BRDFs this maximal value is reached at $\mathbf{k}_1 = \mathbf{n}$, so only one integral has to be computed in practice.

In the following sections, we demonstrate the behavior of the proposed model in more detail and discuss its suitability for different applications.

3 Handling Measured Data

The most obvious way to use d-BRDF framework is, of course, to create new well-behaved BRDFs from user-specified distributions. However, if sufficiently high quality measurement data for a given material are available, a simple procedure exists to extract the necessary distribution from such data. In our experiments we used a representative sample of 13 different materials from Matusik et al. [2003] dataset. This selection covers a broad range of materials from highly specular to very diffuse and contains several paints, metals, plastic and fabrics. Even though there is some anisotropy in the data, we believe that it is mostly due to variation across the sample which should be handled through separate mechanisms (such as textures) and treat all materials as isotropic. However, the procedure described below is equally applicable to anisotropic data and we present it for such general setting.

To extract $p(\mathbf{h})$ from measured data, we note that for backscattering geometry $\mathbf{k}_1 = \mathbf{k}_2 \equiv \mathbf{k}$ we have $\mathbf{h} = \mathbf{k}$ and d-BRDF takes the form

$$\rho_{bs}(\mathbf{k}) \equiv \rho(\mathbf{k}, \mathbf{k}) = \frac{cr_0 p(\mathbf{k})}{2(\mathbf{kn}) - (\mathbf{kn})^2} \quad (6)$$

We can see that after multiplying $\rho_{bs}(\mathbf{k})$ by $2(\mathbf{kn}) - (\mathbf{kn})^2$ we can obtain a function proportional to the distribution $p(\mathbf{k})$. Note that we actually get three separate functions, one for each color channel. If a specific material is well represented by a single d-BRDF, these three functions should have the same shape but can differ by a constant (see Figure 4). One can then simply compute ratios of color components (say, green/red and green/blue) and average the three functions using these ratios as weights. After normalization, we obtain the distribution $p(\mathbf{h})$. The Fresnel parameter r_0 cannot be determined from backscattering data alone, but this value can be estimated from the additional gain in strength $1/r_0$ of the specular highlight at close-to-grazing angles compared with normal incidence. Note that the ratio of color components or r_0 , can be taken to be the same as that of the data, so only a single number has to be determined. Therefore, in practice, we simply render a few images with different r_0 and choose the one giving the best visual match to the original data. One could, of course, perform a numerical fit to the data to obtain the “best” value of r_0 but it is more complex and

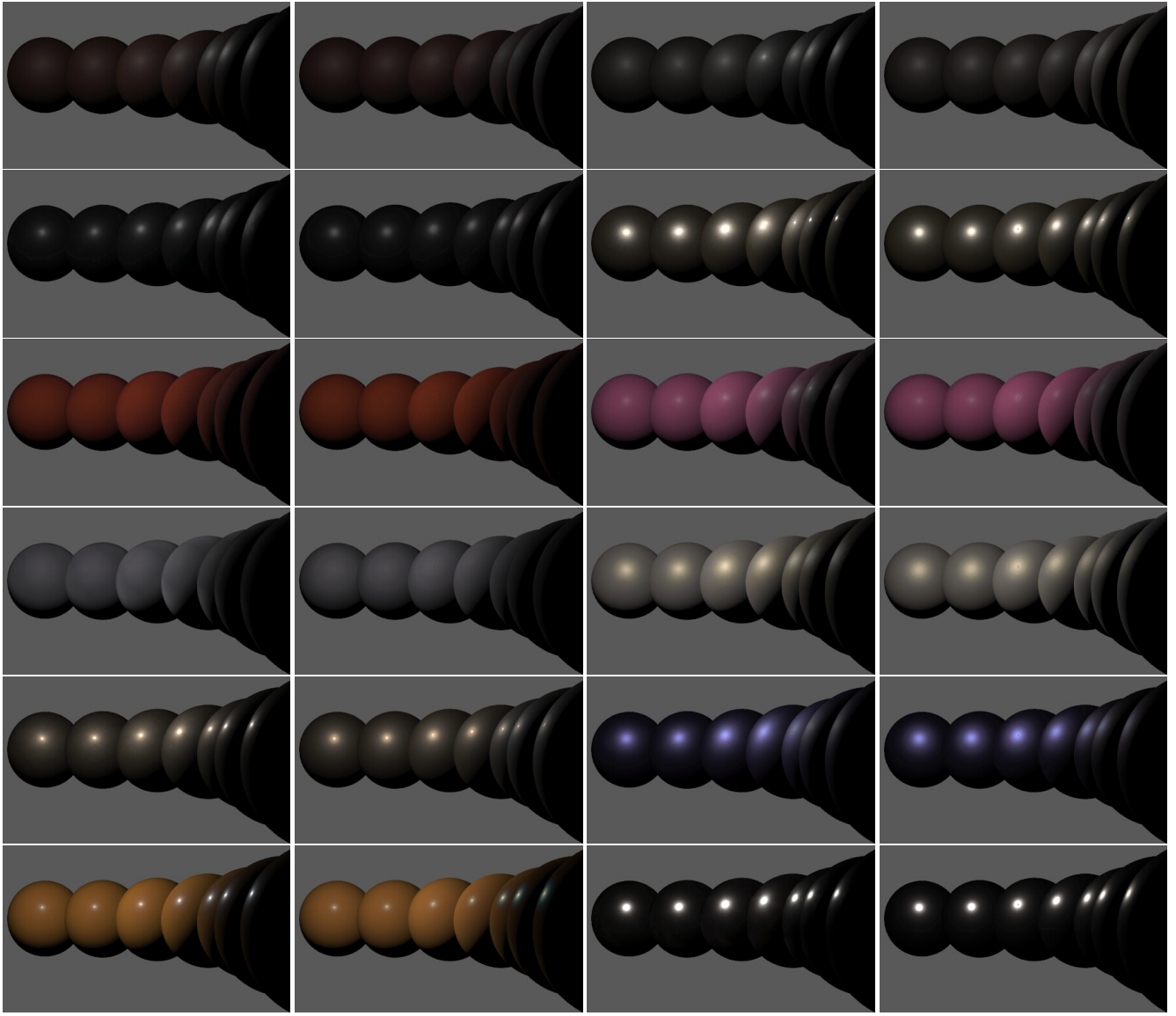


Figure 5: Measured BRDFs (left) and corresponding d-BRDFs (right). First column, from the top: leather; synthetic fabric; fabric 1; fabric 2; aluminum-bronze; plastic. Second column, from the top: oxidized steel; metallic gold; resin; pearl paint; metallic blue paint; nickel. Sphere positions with respect to light were chosen to reduce saturation of specular highlights close to grazing angles. No attempt was made to smooth either measured data or extracted distributions. For all materials except "plastic", no explicit diffuse term was used.

we do not believe that the overall appearance will be significantly improved.

If backscattering functions for different color channels deviate significantly from being just scaled versions of one another, diffuse component of ρ_{bs} should be subtracted out first which corresponds to the standard diffuse+specular separation. It is easy to do so by looking at the region outside the specular peak. If diffuse component is assumed to be Lambertian, it is sufficient to just take the average value in this region as that of BRDF. For the non-Lambertian diffuse, a specific functional form should be chosen. For the single case we encountered which required such processing (plastic), the simple function $\rho_d(\mathbf{k}_1, \mathbf{k}_2) = d_0 + d_1(\mathbf{h})$ with two constants d_0 and d_1 gave a good match but we do not have sufficient data to recommend it as a general solution. Somewhat surprisingly, **for all other materials** the simplest procedure was sufficient, i.e., we did not separate out any special diffuse term, not even a Lambertian one. Results are shown on Figure 5 where side-by-side comparisons of measured BRDF with corresponding d-BRDF are shown for a simple scene of several spheres under single small light inspired by the scene in [Stark et al. 2005]. Note that all spheres are

shown in positions far from backscattering geometry. While some differences can be observed, the overall agreement is quite remarkable given the variety of material properties and the simplicity of the model. As with most models, differences are the largest close to grazing angles but one should remember that typically the data are also least reliable there. Figure 6 shows a numerical comparison of the model results with measured data for metallic blue paint material. The plots use logarithmic scale which is generally accepted to better correspond to visual difference than a linear one. We still believe that visual comparisons of the type presented on Figure 5 carry much more practical information than any fitting error numbers.

Compared to previous approaches, there are no complex or potentially unstable numerical fitting procedures, and $p(\mathbf{h})$ is read almost directly from the data. The resulting representation is very compact: we use just 250 samples for the extracted distributions for isotropic materials we tried, but fewer samples per dimension is certainly possible if a 2D distribution is to be represented. Unfortunately, no truly anisotropic materials were present in the dataset. Furthermore, if necessary, the extracted distribution can be smoothed (and

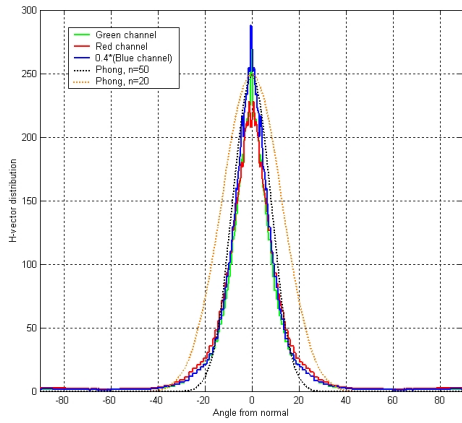


Figure 4: Backscattering data for metallic blue material. Different color channels are very close to being scaled versions of one another. Cross-section through the distribution is plotted for clarity (data for negative angles obtained by symmetry). Unnormalized Phong distributions with $n = 50$ and $n = 20$ are also shown.

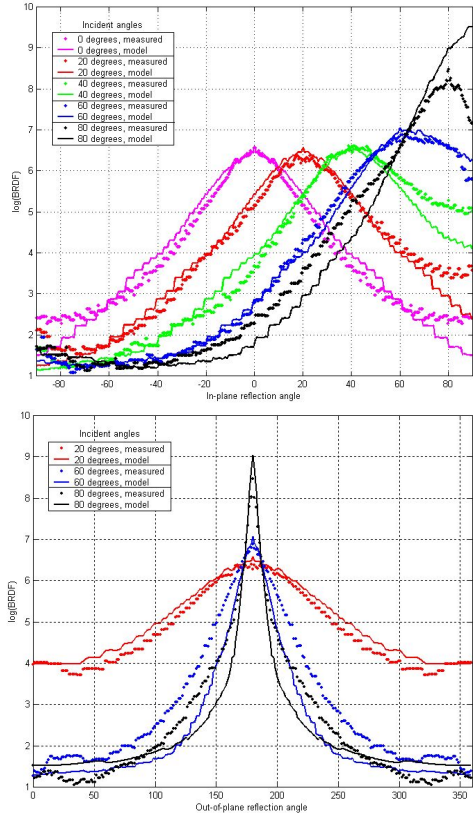


Figure 6: Measured data for metallic blue material compared with d-BRDF values for different incident angles. Distribution was extracted directly from backscattering data. Top: scattering in the plane of incidence (θ_2 -dependence for $\phi_2 = \pi$). Bottom: ϕ_2 -dependence for constant θ_2 in the mirror direction ($\theta_2 = \theta_1$). Blue channel is shown on all plots.

further compressed) by any standard techniques, for example by fitting it with polynomial splines for isotropic materials or spherical harmonics for anisotropic ones. This is much easier to do for

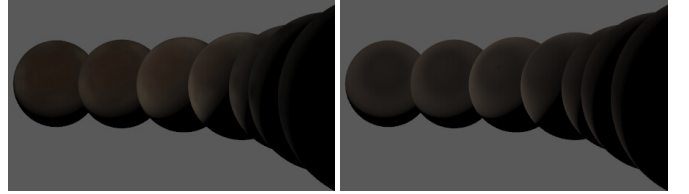


Figure 7: Measured velvet BRDFs (left) and d-BRDFs constructed from $p(\mathbf{h}) = c_{norm}(1 + 4 \exp(-\text{ctan}(\theta)^2))$ distribution (right). Direct reconstruction of the distribution failed for this material.

the lower dimensional function $p(\mathbf{h})$ than for the original BRDF. Note that we do not have to use backscattering data to extract $p(\mathbf{h})$. Instead, data for any other incident angle can provide information about some part of $p(\mathbf{h})$ after corresponding processing. Combining such data for several incident angles will give a complete $p(\mathbf{h})$. One advantage of using backscattering data is that the distribution is read completely and most directly from it and distribution shape is not distorted by the Fresnel term with unknown r_0 .

3.1 Implications for future measurement systems

To represent a material’s full BRDF in our framework, we need only the backscattering data. This represents tremendous reduction in the amount of data which needs to be collected if the d-BRDF representation is acceptable for a given material. We do acknowledge, however, that measuring in this part of the domain is difficult with existing systems. The Matusik et al. [2003] dataset is the only existing one in computer graphics containing sufficiently reliable backscattering data. Even for this excellent dataset, it was clear upon close examination that significant part of inaccuracies one can see on Figure 6 is due to problems with the data rather than inadequacy of d-BRDF representation. The velvet-like fabric shown on Figure 7 demonstrates the extreme case of this. An attempt to extract the distribution from the measured backscatter data directly through the process described above failed to produce any reasonable result for this example. However, a good visual match to this material was still obtained with a d-BRDF using simple “inverted Gaussian with background” distribution [Ashikhmin et al. 2000] $p(\mathbf{h}) = c_{norm}(1 + 4 \exp(-\text{ctan}(\theta)^2))$ where θ is the angle between \mathbf{h} and surface normal. Another, more common, problem we encountered for highly specular materials is a typically broader and less intense specular highlight for backscattering than for any other geometry which is due to geometric limitations on how close the light source and the detector can be positioned.

To remove some of these problems, we believe that it is worth the effort to consider a special system for measuring backscattering. Since the light source and the detector for this geometry have to be close (in direction) and, more importantly, do not have to move with respect to each other, we believe that the resulting device is inherently more compact (and cheaper) than present systems. In fact, a common consumer camera with a built-in flash can serve as such a device. Although there is some separation between the lens and the flash, the fact that we were able to directly use Matusik’s data, which were measured with at least 5 degrees separation between the source and the detector, demonstrates that exact backscattering configuration is not crucial. A *single*, possibly high dynamic range, picture of known curved geometry (a cylinder is sufficient for isotropic materials) then provides enough data to extract the distribution. r_0 can then be estimated from the gain in highlight strength near grazing angle or from general considerations regarding particular material. We are not aware of any simple (i.e. not

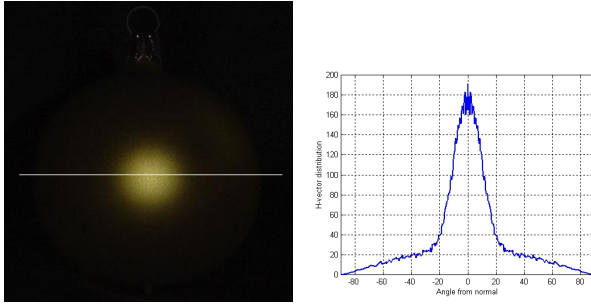


Figure 8: A slice through the center of a photograph (left) provides sufficient information to extract a distribution (right) which can be used to create a d-BRDF approximation, see the last image on Figure 1.

involving special-purpose measurement devices or radiometric calibration with known materials or light sources) technique to obtain *absolute* values for quantities related to light energy (luminance, irradiance, etc.) which are necessary to obtain the correct scaling factor c . However, in most applications it is common to set the overall scaling factor by hand anyway.

As a proof-of-concept experiment, we extracted a distribution from a low dynamic range photograph of a Christmas decoration shown on Figure 8. A single slice through the center of the ball was used. No correction for flash position or data smoothing were applied (except for averaging together left and right halves of the slice to obtain a symmetric distribution). The distribution was then used to render the image shown last on Figure 1 which presents satisfactory visual match to the real material. We believe that high dynamic range photography [Debevec and Malik 1997] combined with better data handling techniques should allow higher quality measurements even with this exceptionally simple technique.

4 Hardware Implementation

The simple mathematical form of our model makes its implementation using modern graphics hardware straightforward with a technique similar to that used for factored representations [Kautz and McCool 1999; McCool et al. 2001]. Specifically, for each material, we create two textures: a two dimensional one to represent $p(\mathbf{h})$ and another one dimensional texture to hold Fresnel fraction $F((\mathbf{kh}))$. In addition, we use a universal auxiliary texture holding the term $(\mathbf{k}_1 \mathbf{n}) / ((\mathbf{k}_1 \mathbf{n}) + (\mathbf{k}_2 \mathbf{n}) - (\mathbf{k}_1 \mathbf{n})(\mathbf{k}_2 \mathbf{n}))$. In our Cg-based implementation, a vertex shader computes all needed texture coordinates given surface normal, light, and view directions. A fragment shader then performs texture lookups into the three textures, multiplies the results together and scales the product by color constant c and light intensity. On most modern architectures multiple texturing units are available and the complete computation can be done in a single pass. Alternatively, simple analytic distributions as well as all other terms can also be evaluated directly inside the shader. The results are shown on Figure 1 and include both analytical distributions and those extracted from measured data as described in the previous section. Analytic examples were chosen to demonstrate versatility of the model and include an anisotropic distribution. It is also demonstrated that a d-BRDF can be easily combined with a separate diffuse (in this case Lambertian) term.

Note that while values stored in Fresnel and auxiliary textures are guaranteed to lie in the $[0; 1]$ interval, this is not the case for distribution $p(\mathbf{h})$. This problem is not unique to our representation and always occurs when high dynamic range data are to be used in hardware. Different solutions have been proposed which range

from simple rescaling and/or clamping (which we use) to more sophisticated techniques [Cohen et al. 2001]. Using a floating point framebuffer combined with a good tone mapping algorithm provides the best, although more complex, solution.

5 Efficient BRDF Sampling

Many modern rendering systems compute radiance leaving the surface through Monte-Carlo integration of the rendering equation [Kajiya 1986] $L(\mathbf{k}_2) = \int L(\mathbf{k}_1)\rho(\mathbf{k}_1, \mathbf{k}_2)(\mathbf{k}_1 \mathbf{n})d\omega_{\mathbf{k}_1}$. The importance sampling technique suggests that one should sample with probability density function (pdf) close in shape to the expression under the integral. However, the incident radiance is typically not known in advance, so sampling according to $\rho(\mathbf{k}_1, \mathbf{k}_2)(\mathbf{k}_1 \mathbf{n})$ is usually the best one can hope to do. One important desirable property of a reflection model is therefore the ability to generate samples with density proportional to (or at least sufficiently close to being proportional to) $\rho(\mathbf{k}_1, \mathbf{k}_2)(\mathbf{k}_1 \mathbf{n})$ for any given \mathbf{k}_2 .

For d-BRDFs we suggest a simple strategy of generating halfvectors \mathbf{h} with density $pdf(\mathbf{h}) = p(\mathbf{h})$ and then reflect the known vector \mathbf{k}_2 around \mathbf{h} to obtain sample direction \mathbf{k}_1 . If \mathbf{k}_1 is below horizon, we set the weight of such a sample to zero. Otherwise, the incoming luminance in the direction of the generated sample is weighted by the standard importance sampling expression

$$\frac{\rho(\mathbf{k}_1, \mathbf{k}_2)(\mathbf{k}_1 \mathbf{n})}{pdf(\mathbf{k}_2)} = \frac{4cF((\mathbf{kh}))(\mathbf{k}_1 \mathbf{n})(\mathbf{kh})}{(\mathbf{k}_1 \mathbf{n}) + (\mathbf{k}_2 \mathbf{n}) - (\mathbf{k}_1 \mathbf{n})(\mathbf{k}_2 \mathbf{n})} \quad (7)$$

where we used relationship $pdf(\mathbf{k}_2) = pdf(\mathbf{h})/4(\mathbf{k}_1 \mathbf{h})$ between pdfs in $\mathbf{h}-$ and \mathbf{k}_2- spaces. To generate samples according to a general numerically represented $p(\mathbf{h})$, we use standard the cumulative density function (cdf) inversion procedure. For an isotropic distribution, we build a 1D cdf table and find \mathbf{h} 's angle θ from the normal by solving $\xi = cdf(\theta)$ where ξ is a random variable uniformly distributed on $[0, 1]$. For better efficiency, we solve this equation beforehand for some number of uniformly spaced ξ values and store the resulting representation of cdf^{-1} function performing just linear interpolation at runtime. The azimuthal angle ϕ is sampled uniformly on $[0, 2\pi]$. Generalization to 2D distributions is straightforward and involves generating separate cdfs for each of a number of θ intervals. To generate an \mathbf{h} sample, one of these intervals is chosen first according to the distribution of total probability concentrated in it. Finally, ϕ is obtained using the corresponding interval-specific cdf. Further factorization into a (sum of) product of 1D factors can be attempted for 2D distributions, but we do not believe that the extra complexity is justified. If material's BRDF is represented by a sum of several terms (for example, two d-BRDFs or a d-BRDF and a Lambertian), the standard strategy is to first choose which term to sample and then generate a sample according to the corresponding distribution. To make the choice, we can precompute directional hemispherical reflectance $R_i(\mathbf{k}_2)$ for each term i , i.e., the fraction of energy incident from a given direction \mathbf{k}_2 which is being reflected. A term is then chosen with probability proportional to its $R_i(\mathbf{k}_2)$. Note that overall pdf also becomes a weighted sum of pdfs of individual terms.

While expression 7 might not suggest this immediately (since ideal weight for luminance sample should be 1), the proposed strategy is actually very efficient, see Figure 9. This can be understood if we recall that the distribution has by far the greatest effect on most aspects of d-BRDF behavior. In fact, for measured data, not only one can sample the d-BRDFs approximation in this manner, but one can sample the *original* BRDF using the same sample generation

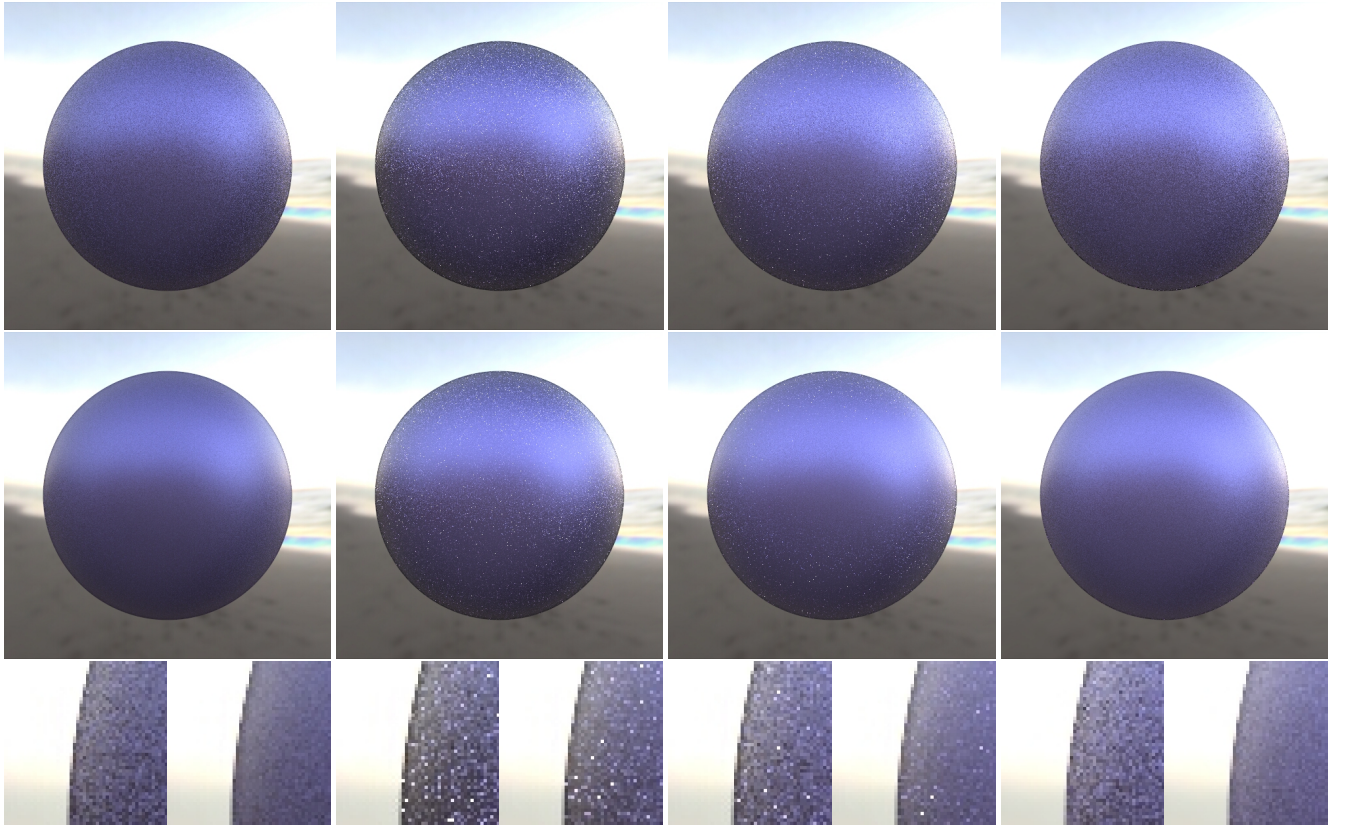


Figure 10: Sampling measured BRDF of metallic blue material with 16 (top row) and 100 (middle row) samples per pixel. From left to right: sampling according to extracted $p(\mathbf{h})$; according to “best fit” Phong distribution ($n = 50$); according to Phong distribution with $n = 20$; sampling using Lawrence et al. factored representation. Because of different tone mapping procedures, overall intensity was adjusted to better match Figure 8 of Lawrence et al.

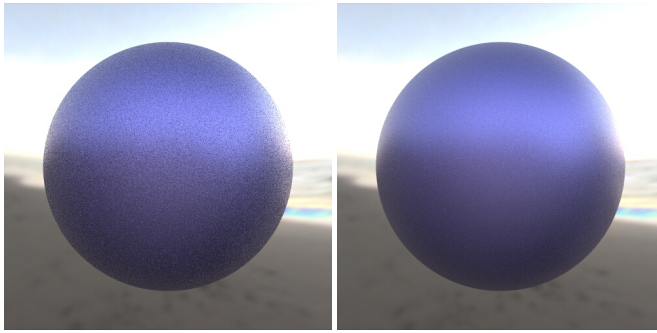


Figure 9: Sampling d-BRDF approximation for metallic blue material. Left: 16 samples/pixel, right: 100 samples/pixel.

procedure but different luminance sample weight

$$\frac{\rho_{\text{measured}}(\mathbf{k}_1, \mathbf{k}_2)(\mathbf{k}_1 \cdot \mathbf{n})}{\text{pdf}(\mathbf{k}_2)} = \frac{4\rho_{\text{measured}}(\mathbf{k}_1, \mathbf{k}_2)(\mathbf{k}_1 \cdot \mathbf{n})(\mathbf{k} \cdot \mathbf{h})}{p(\mathbf{h})} \quad (8)$$

where ρ_{measured} is the original BRDF. Complex analytical models (such as Cook-Torrance) can be sampled in a similar manner once an appropriate distribution is extracted from backscattering data¹.

¹This is the most general strategy effectively treating an analytic model as a measured one. For some models, a better distribution can probably be obtained using advanced knowledge about model details.

The result for metallic blue material is shown in the left column of Figure 10.

The key advantage of the d-BRDF over most other simple models is that it does not restrict the distribution to any specific shape such as Phong or gaussian. In many cases, the deviation of real distributions from these standard functions is quite significant. For example, the distribution on Figure 4 has a sharper central part and broader tails than either Phong or gaussian. This discrepancy directly translates into reduced sampling efficiency. Next two columns of Figure 10 show the results of sampling according to Phong distribution $p(\mathbf{h}) = (n+1)/(2\pi)\cos^n(\theta)$ with $n = 50$ and $n = 20$. For this isotropic material this is the same as sampling according to A&S model. The rightmost column of Figure 10 shows the results obtained with the Lawrence et al. [2004] procedure using the data available online for this material. Because of the apparently different tone mapping procedures used, for all images on Figures 9 and 10 we multiplied the material BRDF by factor of 10 to facilitate direct comparison with Figure 8 of [Lawrence et al. 2004]. Figure 11 shows a more complex scene with global illumination which uses many materials including measured data and Cook-Torrance model. For both examples, we obtain sampling efficiency similar to that of factored representation at a small fraction of the complexity. Interestingly, while plastic material required special processing (separation of a non-Lambertian diffuse term) if a d-BRDF is to replace measured data, to obtain a distribution useful for sampling original BRDF, it was sufficient to follow the most basic extraction procedure with no separate diffuse term at all.

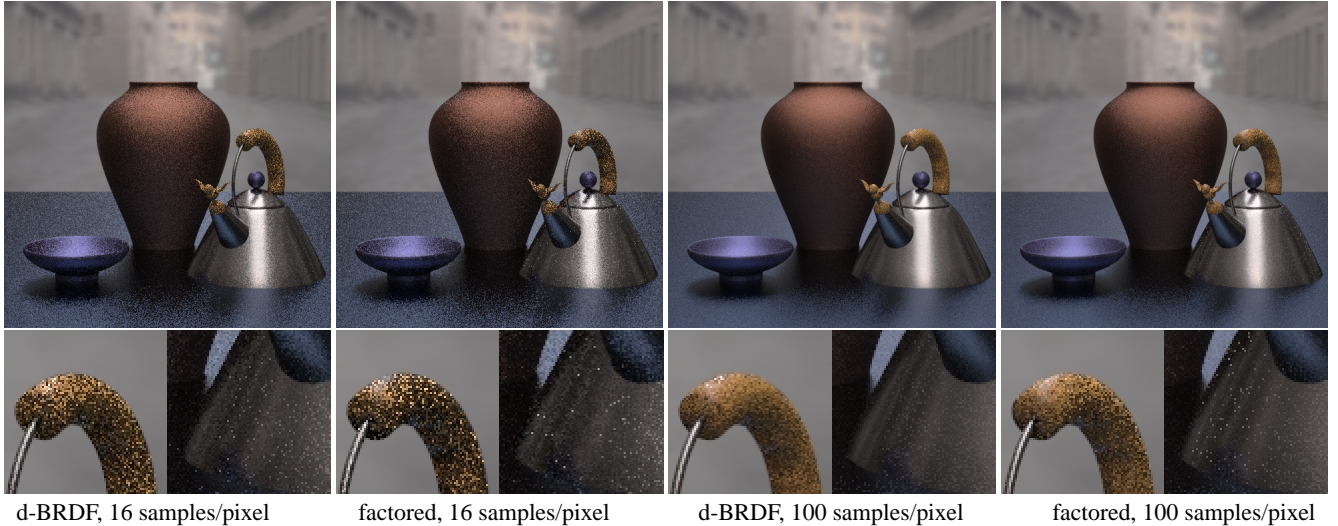


Figure 11: A scene with global illumination rendered with our technique compared with factored representation of Lawrence et al. Materials of the table and the vase are represented by Cook-Torrance model while the bowl and the teapot use measured data (metallic blue, plastic, and nickel). 16 and 100 samples/pixel were used. Paths up to five bounces long were included.

As a side-note, we would like to mention that since the shape of Phong distribution is noticeably different from the real one, sampling with the “best-fit” Phong distribution does *not* generally lead to the least noise. This is because such distribution undersamples parts of the domain where significant density is present, see Figure 4. Since it is still possible to generate samples there (i.e., the pdf is small but not vanishing), the weight of such sample $\rho_{\text{measured}}(\mathbf{k}_1 \mathbf{n})/\text{pdf}$ is extremely large leading to huge contributions to pixel value. These spikes are very hard to “level out” by further sampling and even at 100 samples/pixel significant noise is obvious for the “best fit” Phong distribution. It is generally better to avoid this situation even at the cost of worse overall match between the real distribution and that used for sampling. Therefore, Phong distribution with $n = 20$, which gives a rather poor overall match but reduces the problem described above, is a significantly better choice for sampling than the “best fit” $n = 50$ distribution. Zimmerman [1998] and Lafourche and Willem [1994] presented similar considerations.

6 Limitations

One should not expect that the reflection properties of *all* materials can be accurately described by our model, or any simple model. The fact that we use a only a single low-dimensional function, specifically that of the halfvector, although very convenient, prevents some effects from being accurately modeled. For example, materials which are designed to act as strong retroreflectors for a range of incident angles (such as those used in highway signs) can not be adequately represented. Effects due to wave properties of light are, of course, also not accounted for. We do believe though that d-BRDFs are adequate for a significant percentage of real-world materials. More general discussion on the subject of BRDF dimensionality reduction is given by Stark et al. [2005] and, from a different perspective, by Matusik et al. [2003].

One can certainly create scenes where the relatively small differences between real material and its d-BRDF become highly noticeable. In particular, since most of differences are concentrated near the grazing angle, an infinite plane under low hanging light scene



Figure 12: Leather buddha under three lights (one shining from the front and one from each of the sides), direct illumination only. Left: measured BRDF. Right: d-BRDF. Agreement between measured data and d-BRDF is the worst for this material. Note that only difference in highlight intensity for side lights is visually noticeable for this complex geometry.

of [Stark et al. 2005] presents such case. If such arrangements are of particular importance for a given application, the d-BRDF presents a unique ability to tailor the distribution to get closer to the needed appearance for specific conditions, most likely at the cost of worsening the agreement in other parts of the domain. As already mentioned, more realistic lighting condition or more complex geometry make a precise BRDF match less crucial (see Figure 12 or compare Figures 9 and 10).

Finally, we caution against too direct a physical interpretation of the proposed model. While its general ideas are traceable to microfacet theory, the details lack a solid theoretical foundation leading to some conceptual problems if a physical interpretation is carried too far. In particular, the best values for the Fresnel parameter r_0 , while always inside the theoretically possible interval $[0, 1]$, often lie outside the rather narrow physically reasonable range for a given material. Leaving the (\mathbf{kh}) term in the denominator of 2 helps to make r_0 values somewhat more sensible, but leads to worse color reproduction near grazing angles. We therefore suggest to think about F as a term controlling normal-to-grazing BRDF gain which simply happens to behave like Fresnel.

7 Conclusion

We presented a simple, yet powerful, BRDF model for visual computer graphics applications based on ideas from microfacet theory. The proposed representation is very flexible and possesses many desirable general properties. It is capable of providing a good approximation for measured reflection data with a simple fitting procedure, can be easily implemented in graphics hardware, and allows efficient sampling in a Monte-Carlo rendering system. Since the model uses only backscattering data to reconstruct the complete BRDF, it also suggests a new economical way of measuring surface reflection.

There are several possibilities for future research related to our model. First, our measurement experiment described in section 3.1 should not be considered as more than a proof of concept. We would like to actually build a system which measures backscattering sufficiently accurately. We believe that this would allow to collect reflection data more quickly and easily than is possible today. Once sufficient data is available, it would be interesting to perform an analysis of distributions similar to that done for full BRDFs by Matusik et al. [2003] to isolate salient features responsible for specific appearance trends. Some common material properties can be incorporated by adding special terms to the model. For example, one designed for backscattering should be useful. Finally, systematic discrepancies between the proposed model and measured data near grazing angles suggest that a better overall model might be possible.

References

- ASHIKHMIN, M., AND SHIRLEY, P. 2001. An anisotropic phong brdf model. *Journal of graphics tools* 5, 2, 25–32.
- ASHIKHMIN, M., PREMOZE, S., AND SHIRLEY, P. 2000. A microfacet-based brdf generator. *Proceedings of SIGGRAPH*, 65–74.
- ASHIKHMIN, M., MARSCHNER, S., SHIRLEY, P., AND STAM, J. 2001. State of the art in measuring and modeling surface reflection. In *Course notes of SIGGRAPH 2001*.
- BLINN, J. F. 1977. Models of light reflection for computer synthesized pictures. *Computer Graphics (Proceedings of SIGGRAPH 77)* 11, 2, 192–198.
- COHEN, J., TCHOU, C., HAWKINS, T., AND DEBEVEC, P. 2001. Real-time high dynamic range texture mapping. *12th Eurographics Workshop on Rendering*, 313–320.
- COOK, R. L., AND TORRANCE, K. E. 1981. A reflectance model for computer graphics. *Computer Graphics* 15, 3 (August), 307–316. ACM Siggraph '81 Conference Proceedings.
- DEBEVEC, P. E., AND MALIK, J. 1997. Recovering high dynamic range radiance maps from photographs. *Proceedings of SIGGRAPH 97*, 369–378.
- GREENBERG, D. P., TORRANCE, K. E., SHIRLEY, P., ARVO, J., FERWERDA, J. A., PATTANAIK, S., LAFORTUNE, E. P. F., WALTER, B., FOO, S.-C., AND TRUMBORE, B. 1997. A framework for realistic image synthesis. *Proceedings of SIGGRAPH 97*, 477–494.
- HE, X. D., TORRENCE, K. E., SILLION, F. X., AND GREENBERG, D. P. 1991. A comprehensive physical model for light reflection. *Computer Graphics* 25, 4 (July), 175–186. ACM Siggraph '91 Conference Proceedings.
- KAJIYA, J. T. 1986. The rendering equation. *Computer Graphics* 20, 4 (August), 143–150. ACM Siggraph '86 Conference Proceedings.
- KAUTZ, J., AND MCCOOL, M. 1999. Interactive rendering with arbitrary brdfs using separable approximations. *Proceedings of 10th Eurographics Workshop on Rendering*, 255–268.
- LAFORTUNE, E. P., AND WILLEMS, Y. D. 1994. Using the modified phong BRDF for physically based rendering. Tech. Rep. CW197, Computer Science Department, K.U.Leuven, November.
- LAFORTUNE, E. P. F., FOO, S.-C., TORRANCE, K. E., AND GREENBERG, D. P. 1997. Non-linear approximation of reflectance functions. *Proceedings of SIGGRAPH 97*, 117–126.
- LAWRENCE, J., RUSINKIEWICZ, S., AND RAMAMOORTHI, R. 2004. Efficient brdf importance sampling using a factored representation. *ACM Transactions on graphics* 23, 496–505. Some data available online at <http://www.cs.princeton.edu/gfx/proj/brdf/fig10/>.
- MARSCHNER, S. R., WESTIN, S. H., LAFORTUNE, E. P. F., TORRANCE, K. E., AND GREENBERG, D. P. 1999. Image-based BRDF measurement including human skin. *Eurographics Rendering Workshop 1999*, 131–144.
- MATUSIK, W., PFISTER, H., BRAND, M., AND McMILLAN, L. 2003. A data-driven reflectance model. *ACM Transactions on graphics* 22, 759–769.
- MATUSIK, W., PFISTER, H., BRAND, M., AND McMILLAN, L. 2004. Efficient isotropic brdf measurement. *Eurographics Symposium on Rendering*.
- MCCOOL, M., ANG, J., AND AHMAD, A. 2001. Homomographic factorization of brdfs for high-performance rendering. *Proceedings of SIGGRAPH*, 171–178.
- NEUMANN, L., NEUMANN, A., AND SZIRMAY-KALOS, L. 1999. Compact metallic reflectance models. *Computer Graphics Forum* 18, 13, 161–172.
- NGAN, A., DURAND, F., AND MATUSIK, W. 2004. Experimental validation of analytical brdf models. *SIGGRAPH Sketches and Applications*.
- NICODEMUS, F. E., RICHMOND, J. C., HSIA, J. J., GINSBERG, I., AND LIMPERIS, T. 1977. Geometrical considerations and nomenclature for reflectance. Tech. Rep. 160, National Bureau of Standards.
- OREN, M., AND NAYAR, S. K. 1994. Generalization of lambert's reflectance model. In *Proceedings of SIGGRAPH '94 (Orlando, Florida, July 24–29, 1994)*, ACM Press, A. Glassner, Ed., Computer Graphics Proceedings, Annual Conference Series, ACM SIGGRAPH, 239–246.
- PHONG, B.-T. 1975. Illumination for computer generated images. *Communications of the ACM* 18, 6 (June), 311–317.
- SCHLICK, C. 1994. An inexpensive BRDF model for physically-based rendering. *Computer Graphics Forum* 13, 3, 233–246.
- STAM, J. 1999. Diffraction shaders. *Proceedings of SIGGRAPH 99*, 101–110.
- STARK, M., ARVO, J., AND SMITS, B. 2005. Barycentric parameterizations for isotropic brdfs. *IEEE Transactions on Visualization and Computer Graphics*. to appear.
- TORRANCE, K. E., AND SPARROW, E. M. 1967. Theory for off-specular reflection from roughened surfaces. *Journal of Optical Society of America* 57, 9, 1105–1114.
- WARD, G. J. 1992. Measuring and modeling anisotropic reflection. *Computer Graphics* 26, 2 (July), 265–272. ACM Siggraph '92 Conference Proceedings.
- WESTIN, S. H., ARVO, J. R., AND TORRANCE, K. E. 1992. Predicting reflectance functions from complex surfaces. *Computer Graphics* 26, 2 (July), 255–264. ACM Siggraph '92 Conference Proceedings.
- ZIMMERMAN, K. 1998. *Density Prediction for Importance Sampling in Realistic Image Synthesis*. PhD thesis, Indiana University.